Viscous sintering kinetics of biopolymer filaments extruded for 3D printing

Laurent Chaunier, Guy Della Valle, Denis Lourdin, Anne-Laure Reguerre, Kévin Cochet, Eric Leroy

Viscous sintering kinetics of biopolymer filaments extruded for 3D printing

Laurent CHAUNIER[*a,b], *Guy DELLA VALLE*[a], *Denis LOURDIN*[a], *Anne-Laure REGUERRE*[a], *Kévin COCHET*[a] *and Eric LEROY*[b]

[a]INRA UR1268 BIA Biopolymers Interactions & Assemblies. 44300 Nantes, France

[b]GEPEA, CNRS, UMR-6144, CRTT, 37 avenue de l'université. 44606 St-Nazaire Cedex, France

[*]laurent.chaunier@inra.fr (corresponding author)

Abstract

The characteristic time for viscous sintering of thermoplastics is an important parameter in industrial processes such as welding, rotational moulding but also additive manufacturing. For Additive Manufacturing by Material Extrusion (AM-ME), it gives information about spreading dynamics. An experimental setup was designed to characterize the viscous sintering of cylindrical filaments (extruded for AM-ME) under controlled thermal conditions. It consists of a small thermally controlled oven, coupled with an image acquisition system to follow-up the coalescing cylinders' cross section shape. The evolution of the bonding angle and the convexity index can be calculated to evaluate the temperature dependence of the characteristic time for viscous sintering and the final sintering quality. This approach was applied to glycerol plasticized zein, a biopolymer formulated for AM-ME processing. A processing window (120-130°C) was identified where a high convexity index is reached within a characteristic sintering time close to that of ABS in AM-ME processing conditions.

Keywords

Image analysis; Material extrusion; Model; Viscous sintering; Zein

1. Introduction

The viscous sintering kinetics of thermoplastic polymers has been a key for the understanding and optimization of widely spread industrial processes such as welding and rotational moulding and more recently 3D printing by Selective Laser Sintering (SLS) [1, 2]. In these processes involving spherical particles, the classical model of Frenkel [3] developed for ceramics (and later corrected by Eshelby [4] to satisfy the continuity equation) was first applied: a Newtonian viscous flow under the action of surface tension between two identical spherical objects of initial radius a_0 [m] is generally assumed (Fig. 1). However, an experimental study on rotational moulding polymers showed limitations of the Frenkel-Eshelby's model [5]. Thus, a modified model was proposed in order to take into account the variation of the radius a during sintering and to extend the description of initial coalescence stages [6]:

$$\frac{d\theta}{dt} = \left(\frac{a_0.\mu}{\Gamma}\right)^{-1} . \frac{2^{-\frac{5}{3}}.\cos(\theta).\sin(\theta).(2-\cos(\theta))^{\frac{1}{3}}}{(1-\cos(\theta)).(1+\cos(\theta))^{\frac{1}{3}}} \qquad \text{(Eq. 1)}$$

Where $a(t)$ [m] and $x(t)$ [m] are respectively the radius of the particles and the radius of the neck (Fig. 1, step 2), which define the bonding angle $\theta(t)$ [rad]:

$$\theta = \sin^{-1}\left(\frac{x}{a}\right) \qquad \text{(Eq. 2)}$$

Eq. 1 is thus governed by the characteristic time for viscous sintering $t_{vs1} = \left(\frac{a_0.\mu}{\Gamma}\right)$ [s]. The surface tension of the polymer melt, Γ [N.m^{-1}], acts as a driving force, whereas the melt viscosity, μ [Pa.s], acts as a limiting one during coalescence.

For sintering of particles of polymers typically used in rotational moulding (HDPE and LLDPE) under isothermal conditions, the numerical solution of Eq. 1 showed significantly better predictions than the Frenkel-Eshelby's model [6]. The experimental data were obtained

using an optical microscope equipped with a temperature controlled heat chamber, to monitor the coalescence of polymer particles placed on a glass plate.

Actually, Eq.1 was later used by its authors to model bond formation between polymer filaments in Additive Manufacturing (AM) by Material Extrusion process (AM-ME, known under the trade name "Fused Deposition Modelling", FDM): The same experimental approach was applied to study the coalescence of thin slices of extruded filaments of ABS, a standard amorphous polymer for AM-ME process, under optical microscope [7]. More recently, a different experimental setup was proposed to study the sintering of real filaments of semi-crystalline thermoplastic polymers dedicated to AM-ME [8]: two extruded filaments are placed in a transparent oven allowing monitoring the coalescence of the filaments upon controlled heating temperature ramps. In this case, images acquisition (1frame/5s) allowed the measurement of the bonding neck as a function of time. Such experiments validated the predictions of the model (Eq. 1) for PLA, the main semi-crystalline polymer used in AM-ME, as well as for PEEK at higher temperature.

However, the application of Eq.1 to model bond formation between polymer filaments in AM-ME is questionable for two reasons:

1) Eq. 1 is supposed to describe the sintering kinetics of spherical particles, not cylindrical filaments. To our knowledge, the only model for the reliable prediction of sintering kinetics for two identical cylinders was proposed by Hopper [9]. This model cannot be expressed in a single differential equation. It is based on the geometrical description of the two cylinders cross section by an inverse ellipse of constant area. The author gives the numerical solution in the form of a table of values of:

$$\left(\frac{\Gamma.t}{\mu.a_0}.\frac{1}{\sqrt{2}}\right) = \left(\frac{t}{t_{vs2}}.\frac{1}{\sqrt{2}}\right) \text{ vs. } \left(\frac{x}{a_0}.\frac{1}{\sqrt{2}}\right).$$

The $\frac{1}{\sqrt{2}}$ factor actually comes from the assumption that after complete coalescence, a single cylinder of radius $a_f = \sqrt{2}.a_0$ is obtained. Compared to the predictions of the

model for spherical particles (Eq. 1) those from Hopper's model for cylinders show similar results at the beginning of sintering, up to $x/a_0 = 0.8$. However, noticeable differences, about 10%, are obtained at the completion of coalescence, with final $x/a_0 = 1.41$ for Hopper's model and $x/a_0 = 1.26$ when applying Eq. 1 [6]. However, Hopper's model was not used in later works on cylinder coalescence [7, 8].

2) Recent experimental [10] and modelling results [11] suggest that viscous sintering is not the main phenomenon involved in bond formation during AM-ME. Infrared thermography measurements [10] during the process showed that the cooling rate of the deposed filaments is extremely fast (≈ 100 °C/min) and that the temperature at the interface between two filaments does not stay above the glass transition temperature more than 1 to 2 s. For that reason, a recent modelling work [11] insists on the role of polymer chain interdiffusion at the interface between filaments (Fig. 1, step 3), which occurs much faster that viscous sintering kinetics described by Eq.1, and is known to be a key phenomenon affecting the final quality of the bond adhesion [12]. However, the same authors point out that their model neglects the polymer spreading dynamics at the filaments interface that necessarily precedes and affects chain interdiffusion [11]. Indeed, it is known that spreading dynamics are governed by a same characteristic time $\left(\frac{a_0 \cdot \mu}{\Gamma}\right)$ [13], that is to say the same characteristic time involved in viscous sintering $t_{vs1}, or\ t_{vs2} = \left(\frac{a_0 \cdot \mu}{\Gamma}\right)$ [s].

Therefore, while studying viscous sintering kinetics of filaments does not mimic the whole complexity of AM-ME, it provides an interesting way to access the temperature dependence of a characteristic time that is of strong interest in the perspective of a detailed understanding and modelling of this process. So, the present work has the following objectives:

- The design of an experimental setup allowing the monitoring of the coalescence of polymer filaments by a camera, at temperatures ranging from the extrusion temperature used in AM-ME, down to significantly lower temperatures.
- The development of an image advanced analysis of the frames taken by the camera to sharply characterize the sintering kinetics.
- The identification of the characteristic time for viscous sintering at different temperatures by modelling the experimental data by both Eq. 1 (spherical particles approximation) and the model of Hopper for cylinders.

This approach is applied to a biopolymer recently pointed out as a candidate for the AM-ME process and formulated in this purpose: Zein, a protein from corn, with potential applications as a biomaterial taking advantage of its bioresorbability [14].

2. Experimental

2.1. Raw materials and plasticized zein processing

Commercial zein in the powdery state (Ref. Z3625, containing 5% moisture) and glycerol, used as a plasticizer, were purchased from Sigma-Aldrich (Saint-Quentin-Fallavier, FR). These materials were mixed in a household kneader (De'longhi Kenwood; Clichy, FR) for 2 min at 20 °C, to obtain the formulation based on zein with 20w% glycerol. This mixture was processed with a twin-screw microcompounder (Haake Minilab, Thermo Scientific GmbH; Karlsruhe, DE) at 130 °C, to extrude the plasticized zein through a cylindrical die ($Ø_{filament}$ = 2 mm). The extruded filaments were cut as cylinders with a constant length, $L_{filament}$ = 5 mm, for subsequent fusion bonding trials. Longer cylinders (20 mm) were also cut for Dynamic Mechanical Analysis.

2.2. Cylindrical filament sintering experimental setup

121 The “hardware” experimental setup (Fig. 2-a) is inspired by the design recently described by
122 Bakrani *et al.* [8] for the sintering of two horizontally adjacent extruded filaments. However,
123 various parameters have been optimized for the specific objectives of the present work:

124 - The internal dimensions of the oven (20 x 10 x 50 mm^3) are significantly reduced.
125 Such a small volume of this thermostated chamber allows rapid heating of the cavity
126 machined in a sole parallelepiped aluminium block. The front of the cavity is a
127 transparent glass plate, while the back is equipped with 3 LEDs ($Ø_{LED}$ = 3.6 mm, 6500
128 K, 39 lm; OSRAM Opto Semiconductors, Regensburg, DE) mounted in series for
129 backlighting the two cylinders.

130 - A great attention was paid to thermal control and monitoring: the oven was equipped
131 with a temperature controller (Model 1/16 DIN with automated PID, 48 x 48 x 100
132 mm^3; RKC Instrument Inc.; Tokyo, JP) and 4 electrical thermal resistances ($Ø_{resistance}$ =
133 6.5 mm and $L_{resistance}$ = 40 mm, P = 30 W each; RS Pro Components SAS, Beauvais,
134 FR) embedded at each of the four corners of the oven. The regulation thermocouple
135 (Type T) was located at the middle of the horizontal upper wall of the oven, in contact
136 with the metal surface. A second thermocouple (type K) was located in the medium
137 part of the oven cavity in order to monitor the environment temperature (T_{oven}, [°C]).

138 - A high image acquisition rate was used (1 frame.s^{-1}): A CMOS camera (EXO model,
139 SVS-Vistek GmbH; Seefeld, DE) equipped with a 20 mm length optical extension and
140 a magnifying lens (Computar model 5.6-32 C macroX10; CBC, Cary, NC, US) has
141 been placed in front of the glass window (Fig. 2-b). This camera allows the acquisition
142 at 1 frame.s^{-1} of contrasted images coded on 8 bits (256 grey levels, as Tagged Image
143 Format files “.TIF”) of the cylinders’ cross section. The resolution was determined
144 with a Vernier calliper for each sintering sequence. The average value was found at
145 150 pixels.mm^{-1}.

146 The experimental procedure involves three successive steps:

147 i) Setting the desired sintering temperature T_{set} on the temperature controller, from 80
148 °C to 140 °C. In this interval, it takes about 7 min to reach a stabilized value $T_{oven} = T_{set} \pm 0.1$
149 °C in the cavity.

150 ii) Introducing the filaments after opening and closing the transparent window. After
151 this opening/closing sequence, the temperature of the cavity slightly decreases but it takes 10
152 to 20 s for the system to stabilize again at $T_{oven} \approx T_{set}$.

153 iii) Starting image acquisition.

154 For each temperature T_{set}, experimental trials have been triplicated. In order to monitor
155 precisely the temperature of the filaments, a fourth series of experiments was performed in
156 which a thin thermocouple (type K, $Ø_{thermocouple} \approx 0.4$ mm) was located inside one of the two
157 filaments, to measure the temperature at the core of the extruded material ($T_{filament}$, [°C]). The
158 filament was finely drilled to its half-length in order to insert the thermocouple tip.

159 *2.3. Image analysis*

160 In the initial images, the section of the two extruded filaments and their fusion bonding neck
161 appear as a dark shape on a bright background (Fig. 2-b). An example of their evolution
162 during a sintering sequence at a temperature $T_{set} = 130$ °C is shown on Fig. 3-a.

163 The successive steps of the image analysis involve: (i) the selection of the region of interest
164 (ROI) by cropping the initial image; (ii) the segmentation by image thresholding carried out
165 with ImageJ (free software; National Institute for Health, US), to obtain binary images with
166 one white object on a black background; (iii) the morphological analysis (implemented on
167 Matlab; The MathWorks Inc., Natick, MA, US).

168 The following morphological descriptors have been defined in order to calculate the bonding
169 angle evolution $\theta(t)$ (Eq. 2):

- The minimum vertical length, L_{Min}, equal to *2.x* (Fig. 1), corresponding to the bonding neck length.

- The two maximum vertical lengths, L_{MaxL} and L_{MaxR}, for the left and right areas, respectively (Fig. 3-b). Their average value, L_{Max}, is used to calculate the equivalent radius of the filaments given by:

$$a = \frac{L_{Max}}{2} = \frac{(L_{MaxL}+L_{MaxR})}{4} \quad \text{(Eq. 3)}$$

Application of Eq. 2 gives the bonding angle:

$$\theta = \sin^{-1}\left(\frac{x}{a}\right) = \sin^{-1}\left(\frac{L_{Min}}{L_{Max}}\right) \quad \text{(Eq. 4)}$$

Additional morphological descriptors were defined in order to calculate a convexity index of the system, I_{Convex} (Fig.3-b):

- The left (S_L) and right (S_R) cylinder's areas.

- The convex area, S_{Convex}, corresponding to the whole object of the segmented images. It includes S_L and S_R, and the concavities between filaments.

A sketch depicting S_L, S_R and S_{Convex} is shown on Fig. 3-b. The convexity index, I_{Convex} [-], is defined as:

$$I_{Convex} = \frac{(S_L+S_R)}{S_{Convex}} \quad \text{(Eq. 5)}$$

I_{convex} reaches the value 1 if the fusion bonding leads to a perfect welding of filaments, without any residual concavity between them [15].

2.4. Characterization of plasticized zein

Dynamic Mechanical Analysis (DMA, Model 50N-O1dB; Metravib, Lyon, FR) was performed on cylindrical filaments. Prior to DMA trials, extrudates were coated with a silicone-based hydrophobic grease to limit their dehydration. The mechanical active length between the two grips was set at 10 mm and the extrudates were characterized in the tensile mode at 1Hz, with a strain set at 0.1 % and heating rate 3 °C.min^{-1}.

3. Results and discussion

The typical evolution of the oven and filament temperatures at the start of sintering experiments is shown on Figure 4. At t = 0, the transparent window is closed and temperature (and image) acquisition is started. As stated in the experimental section, it typically takes 10 to 20 s for T_{oven} to come back to the regulated T_{set} value. However, it can be seen that it takes more time for the filament core to heat up. It was assumed that the system reached steady state for (T_{oven} - $T_{filament}$) < 5 °C. Typically that corresponds to 35 s at 130 °C, slightly higher than the value of 15 to 20 s, reported in the case of thermomicroscopy trials at 190 °C on thermoplastic particles (Ø ≈ 0.5 mm) between glass plates [5].

The time dependences of the bonding angle and the convexity index obtained from image morphological analysis are plotted on Figure 5. In order to compare the sintering rates at different temperatures, the slopes $d\theta/dt$ [$rad.s^{-1}$] were evaluated for t = 35 s (Table 1). This time was chosen on the basis of filament temperature measurements to ensure isothermal steady conditions (Fig. 4). The maximum (final) values of the convexity index (I_{convex_final}) are also reported in Table 1. Three different behaviours can be depicted:

- For the lowest temperatures (80 °C and 100 °C), the sintering kinetics are very slow ($d\theta/dt$ about 3.10^{-4} $rad.s^{-1}$ and 28.10^{-4} $rad.s^{-1}$, respectively; Table 1) and sintering is far from being complete even for long residence times: the final convexity index values, close to 0.9, are reached after more than 800 s (out of the plot range). This means that the concavities between the sintered filaments still represent 10 % of the cross section surface, with final bonding angles remaining low (θ_{final} < 0.4 and 0.8 rad, respectively; Table 1).

- For the highest temperature (140 °C), sintering appears very fast ($d\theta/dt$ > 0.06 $rad.s^{-1}$) (Fig. 5-a and Table 1). However, the convexity index curve (Fig. 5-b) suddenly drops around 30 s. This drop reflects an expansion of the material due to the formation of bubbles

because of plasticizer vaporization. The induced variations in filament dimensions lead to a jagged bonding angle curve (Fig. 5-a). It also has to be noted that the values plotted are average values, whereas the standard deviations are very large in this case (Table 1).

- In the interval [120, 130°C], the maximum (final) values of the convexity index are close, from 0.972 to 0.987, indicating an almost perfect sintering without residual concavity and high final bonding angle, θ_{final} > 1 rad (Table 1). The time necessary to reach this final state decreases with temperature, while sintering rates show a threefold increase (from about 0.011 to 0.036 rad.s^{-1}).

These results illustrate the significance of the convexity index obtained from morphological analysis, as a sensitive indicator of the temperature dependence of the sintering quality. It allows detecting expansion problems at higher temperatures, and residual concavity at lower ones.

The values of θ and dθ/dt at t = 35s in Table 1 can be used to evaluate the characteristic time for viscous sintering t_{vs1} simply by using Eq. 1 [6]. The same determination with Hopper's model [9] requires the calculation of a master curve (Fig. 6): On this curve (dθ / d(t/t_{vs2})) is plotted as a function of θ. The values were calculated from the numerical data $\left(\frac{\Gamma.t}{\mu.a_0}.\frac{1}{\sqrt{2}}\right) = \left(\frac{t}{t_{vs2}}.\frac{1}{\sqrt{2}}\right)$ *vs.* $\left(\frac{x}{a_0}.\frac{1}{\sqrt{2}}\right) \approx \left(\sin\theta\,.\frac{1}{\sqrt{2}}\right)$ given in Hopper's article. For each temperature, taking the value of θ at t = 35 s, the value of t_{vs2} is given by the following relation after reporting our experimental data on the master curve:

$$\left(\frac{d\theta}{d\left(\frac{t}{t_{vs2}}\right)}\right) = t_{vs2}.\left(\frac{d\theta}{dt}\right) \qquad \text{(Eq. 6)}$$

The comparison of the characteristic times for viscous sintering obtained with Eq. 1 and Hopper's model master curve, given in Table 1 as the ratio t_{vs1}/t_{vs2}, shows that, except for the lower temperatures (80-100 °C), the assumption that cylinders sintering can be modelled by Eq. 1 developed for spherical particles is quite reasonable.

We have reported the values of the characteristic time for viscous sintering obtained using the Hopper's model, t_{vs2}, on Figure 7. The processing window for fast sintering in AM-ME is shown as a grey area. Figure 7 also shows the main mechanical relaxation associated to the glass transition of plasticized zein filament observed in DMA. At 25 °C, the material is in the glassy state, with a storage modulus E′ close to 1 GPa. This modulus decreases with temperature, taking values close to the loss modulus E″ which displays a maximum at $T_{peak\_E''}$ ≈ 45 - 48 °C, close to the glass transition temperature previously determined by differential scanning calorimetry, T_g = 42 °C for the same composition [16]. Beyond 75-80 °C, the moduli measurements become unreliable due to creeping. Actually, in a previous rheological study on zein plasticized by glycerol, we showed that in this temperature range, the material starts to flow, under shear, the loss modulus being higher than the storage modulus [16]. For lower temperatures, above the relaxation associated to the glass transition, sintering is still possible, but slow, with characteristic times much larger than 100 s. For higher temperatures, at 140 °C, the expansion of the material ascribed to plasticizer evaporation perturbs the coalescence. Finally, in the 120-130 °C range, corresponding to T_g + 80-90 °C, the estimated characteristic time for viscous sintering decreases from 82 s to 25 s.

The values obtained for the viscous sintering of plasticized zein melt can be compared to those of ABS at its AM-ME processing temperature T = 240 °C. Assuming $|\eta^*|_{ABS\_240°C}$ = 5100 Pa.s, $\Gamma_{ABS\_240°C}$ = 29 mN.m^{-1} and $2.a_{0\_ABS\_240°C}$ = 0.47 mm [7, 17], we obtain $t_{vs\ ABS\_240°C}$ ≈ 41 s. This value is very close to the one estimated in this study for the characteristic sintering time of plasticized zein. In previous studies, the processability of plasticized zein by AM-ME was first ascribed to its rheological behaviour at 120-130 °C [16], similar to that of ABS at 230-270 °C. This similarity is confirmed for the characteristic time for viscous sintering and suggests that the values of surface tension of the two polymers in the molten state are also close.

In future works, the experimental design and image morphological analysis system described in the present study could be used to characterize the viscous sintering behaviour of other materials, and especially those developed for AM-ME. Moreover, in the present work, we considered only the shape evolution of the two cylinders cross section. As pointed out in the introduction, the quality of the bond obtained by sintering involves polymer chains interdiffusion through the bonding interface (Fig. 1, step 3). The experimental device may actually be used to produce samples for variable sintering times, in order to test the evolution of adhesion with time and temperature.

4. Conclusions

An experimental setup has been designed for the characterization of viscous sintering between two polymer cylinders. It consists of a small thermally controlled oven, coupled with an image acquisition system. The coalescing cylinders' cross section shape is determined as a function of time by morphological analysis. The two key variables monitored are the bonding angle and the convexity index. The knowledge of the evolution of the bonding angle allows quantifying the temperature dependence of the characteristic time for viscous sintering, t_{vs}, while the convexity index, I_{convex}, is shown to be a sensitive indicator of the temperature dependence of the sintering quality.

This approach is illustrated in the case of glycerol plasticized zein, a biobased thermoplastic material formulated for Additive Manufacturing by Material Extrusion (AM-ME). A narrow processing window (120-130 °C, corresponding to T_g + 80-90 °C) is identified using the values of t_{vs} and I_{convex} obtained at different sintering temperatures. In this window, the value of t_{vs} for glycerol plasticized zein is close to the one of ABS at its typical AM-ME processing temperature.

293 **Acknowledgements**

294 The authors would like to thank Yannick Madec (University of Nantes, Carquefou), David
295 Legland, Patrice Papineau and Roselyne Désirest (INRA, Nantes) for helpful discussions and
296 experimental support.

297 **References**

298 [1] J. Boyd, W.T.J. West, S. Wu, E.S. Takacs, J. Vlachopoulos, M.R. Thompson, Automated
299 image analysis to characterize the melt densification stage of polymer sintering processes,
300 Polymer Testing 60 (2017) 242-249.
301 [2] L. Xin, M. Boutaous, S.H. Xin, D.A. Siginer, Multiphysical modeling of the heating phase
302 in the polymer powder bed fusion process, Additive Manufacturing, 18, (2017).121-135.
303 [3] J. Frenkel, Viscous flow of crystalline bodies under the action of surface tension, Journal
304 of Physics (USSR) 9 (1945) 385- 391.
305 [4] J. Eshelby, Discussion of 'Seminar on the Kinetics of Sintering'. Metallurgical
306 Transactions 185 (1949) 796–813.
307 [5] C.T. Bellehumeur, M.K. Bisaria, J. Vlachopoulos, An experimental study and model
308 assesment of polymer sintering. Polymer Engineering and Science 36(17) (1996) 2198-2207.
309 [6] O. Pokluda, C.T. Bellehumeur, J. Vlachopoulos, Modification of Frenkel's Model for
310 Sintering, AIChE Journal, 43(12) (1997) 3253-3256.
311 [7] C. Bellehumeur, L. Li, Q. Sun, P. Gu, Modeling of bond formation between polymer
312 filaments in the fused deposition modeling process, Journal of Manufacturing Processes 6
313 (2004) 170-178.
314 [8] S. Bakrani, F. Chabert, V. Nassiet, A. Cantarel, C. Garnier, Toward improvement of the
315 properties of parts manufactured by FFF (Fused Filament Fabrication) through understanding
316 the influence of temperature and rheological behaviour on the coalescence phenomenon, AIP
317 Conference Proceedings 1896, 040008 (2017), doi: 10.1063/1.5008034.
318 [9] R.W. Hopper, Coalescence of Two Equal Cylinders: Results for Creeping Viscous Plane
319 Flow Driven by Capillarity, Communications of the American Ceramic Society (1984) C262-
320 C264.

[10] J.E. Seppala, K.D. Migler, Infrared thermography of welding zones produced by polymer extrusion additive manufacturing, Additive Manufacturing 12, Part A (2016) 71-76.

[11] C. McIlroy, P.D. Olmsted, Disentanglement effects on welding behaviour of polymer melts during the fused-filament-fabrication method for additive manufacturing, Polymer 123 (2017) 376-391.

[12] C.A. Butler, R.L. McCullough, R. Pitchumani, J.W. Gillespie, An analysis of mechanisms governing fusion bonding of thermoplastic composites, Journal of Thermoplastic Composite Materials 11(4) (1998) 338-363.

[13] R.S. Crockett, P.D. Calvert, The liquid-to-solid transition in stereodeposition techniques, 7th Solid Freeform Fabrication (SFF) Symposium, Univ Texas Austin, Conference Proceedings, (1996) 257-264.

[14] L. Chaunier, S. Guessasma, S. Belhabib, G. Della Valle, D. Lourdin, E. Leroy, Material extrusion of plant biopolymers: opportunities & challenges for 3D printing, Additive Manufacturing 21 (2018) 220-233.

[15] D. Legland, J. Beaugrand, Automated clustering of lignocellulosic fibres based on morphometric features and using clustering of variables, Industrial Crops and Products 45 (2013) 253-261.

[16] L. Chaunier, G. Della Valle, M. Dalgalarrondo, D. Lourdin, D. Marion, E. Leroy, Rheology and structural changes of plasticized zeins in the molten state, Rheologica Acta 56(11) (2017) 941-953.

[17] Q. Sun, G.M. Rizvi, C.T. Bellehumeur, P. Gu, Effect of processing conditions on the bonding quality of FDM polymer filaments, Rapid Prototyping Journal 14(2) (2008) 72-80.

343 **Figure captions**

344 **Figure 1.** Fusion bonding steps at high temperature between two model circular thermoplastic
345 particles: 1- intimate contact, 2- apparition of a bonding neck, 3- neck growth due to polymer
346 diffusion through interface and 4- randomization for long time.

347

348 **Figure 2.** Scheme and photos of the experimental sintering device to follow up the
349 coalescence of polymer cylinders: (a) Thermally regulated oven (20 x 10 x 50 mm^3) equipped
350 with an internal backlighting and a CMOS camera with magnifying lens for image
351 acquisition. (b) Photos of the experimental device and example of cylinders' cross section
352 initial image, at t = 0 s, of a sintering sequence between two zein-based extruded filaments at
353 130°C with $Ø_{filament}$ = 2 mm.

354

355 **Figure 3.** Successive steps presented for some selected images acquired during 60 s of a
356 typical sintering sequence at 130°C between two zein-based extruded filaments: (a)
357 Acquisition of images in 256 grey levels; after selection of the Region Of Interest (ROI),
358 segmentation by thresholding (binary image); pre-treated images ready for the morphological
359 analysis with the automated identification of each of the two initial filaments sections. (b)
360 Sketch depicting the morphological descriptors S_L, S_R and S_{Convex} used for the calculation of
361 the convexity index, I_{Convex} (Eq. 5).

362

363 **Figure 4.** Evolutions of the temperatures in the oven and at the core of zein-based extruded
364 filaments for T_{set} = 80°C, 100°C and 130°C.

365

366 **Figure 5.** Evolutions of the bonding angle, θ [rad], (a) and the convexity index, I_{convex} [-], (b)
367 during the sintering of two zein-based extruded filaments at different temperatures.

Figure 6. Master curve for the Hopper's model and experimental points.

Figure 7. Thermomechanical properties of a zein-based extruded filament assessed by DMA (E′, the storage modulus [Pa] and E″, the loss modulus [Pa]) and average characteristic time for viscous sintering using the Hopper's model (from Table 1). Peak of the loss modulus, E″, is indicated by a black vertical arrow and the processing window by AM-EM is represented as a grey area.

376

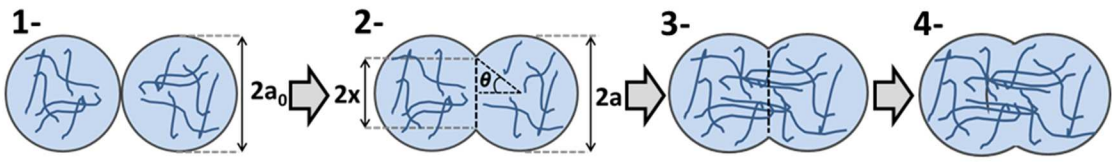

377

378 **Figure 1.** Chaunier *et al.*

379

a-

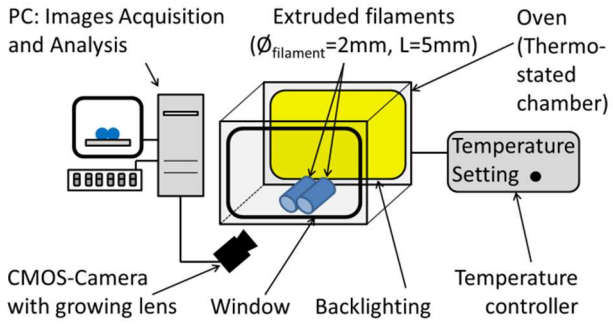

b-

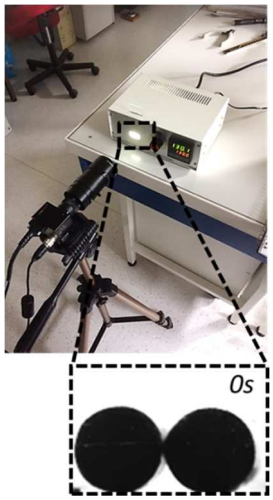

380

381 **Figure 2.** Chaunier *et al.*

382

a-

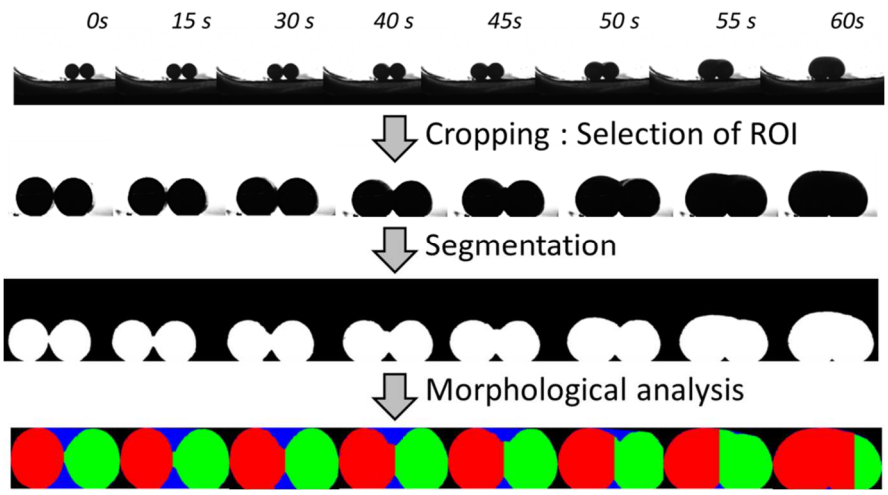

b-

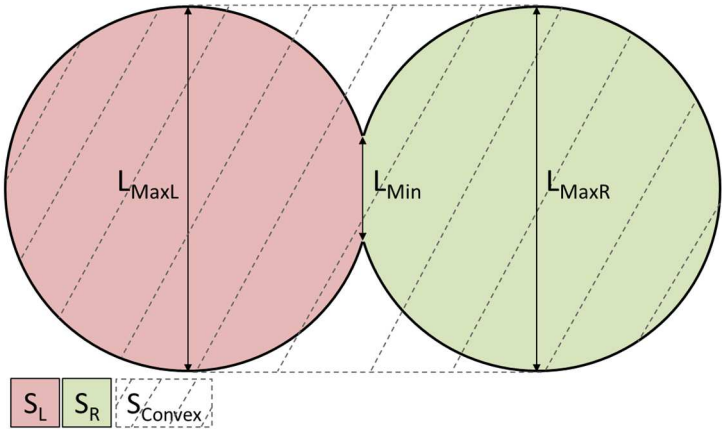

Convexity Index calculation: $I_{Convex} = \frac{(S_L+S_R)}{S_{Convex}}$ (Eq. 5)

383

384 **Figure 3.** Chaunier *et al.*

385

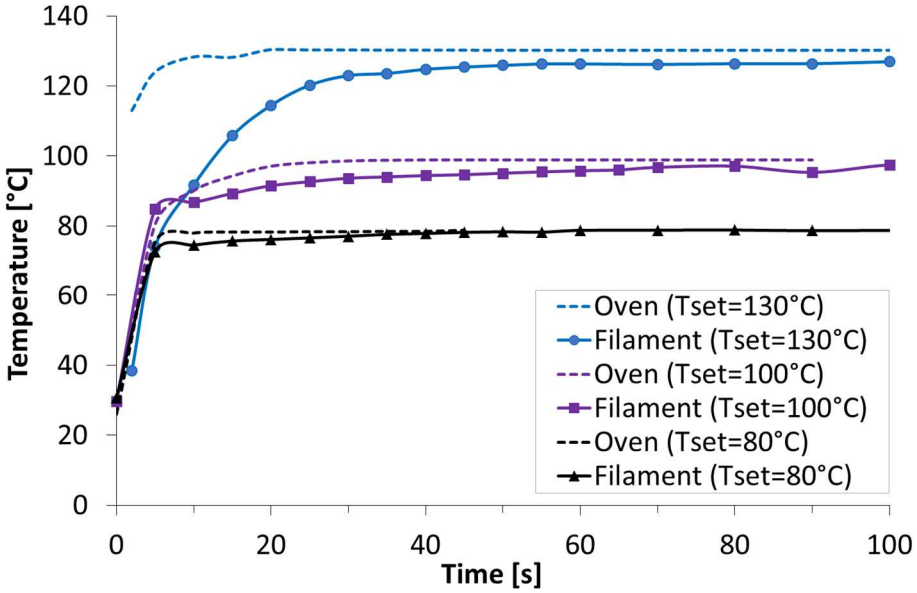

386

387 **Figure 4.** Chaunier *et al.*

388

a-

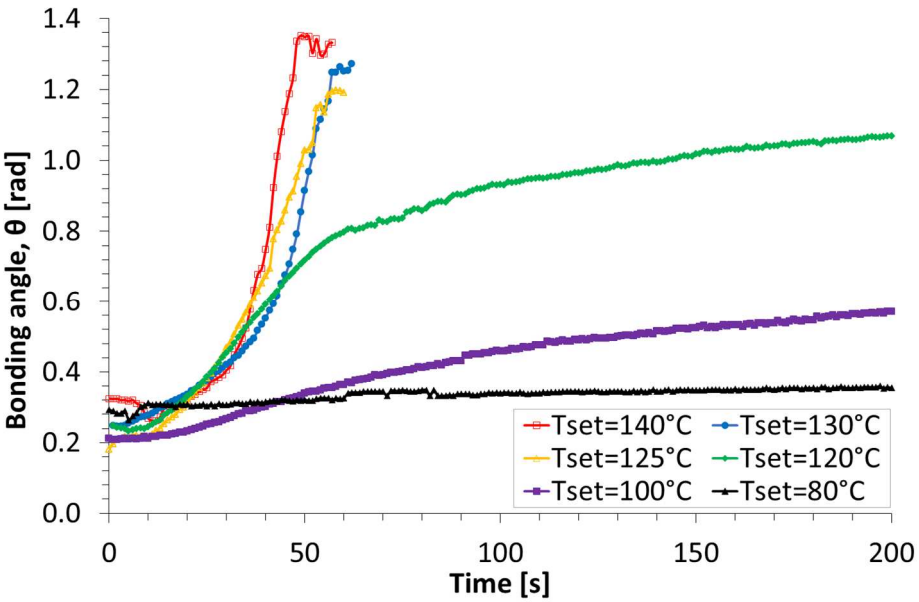

b-

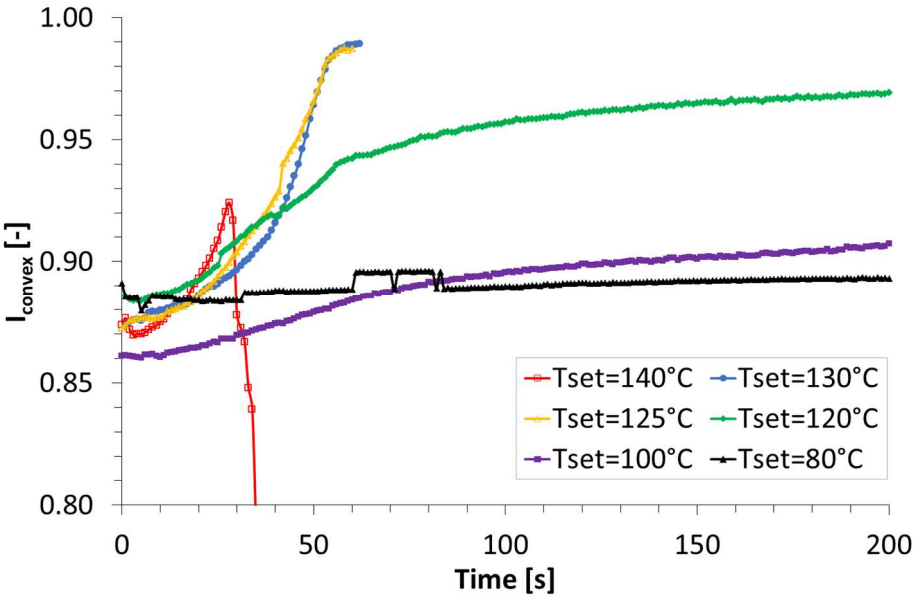

389

390 **Figure 5.** Chaunier *et al.*

391

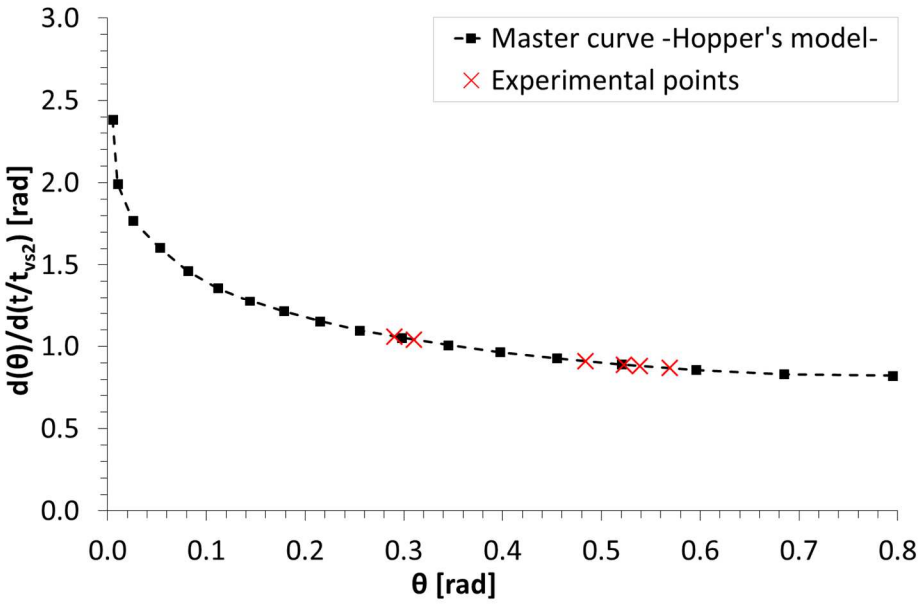

392

393 **Figure 6.** Chaunier *et al.*

394

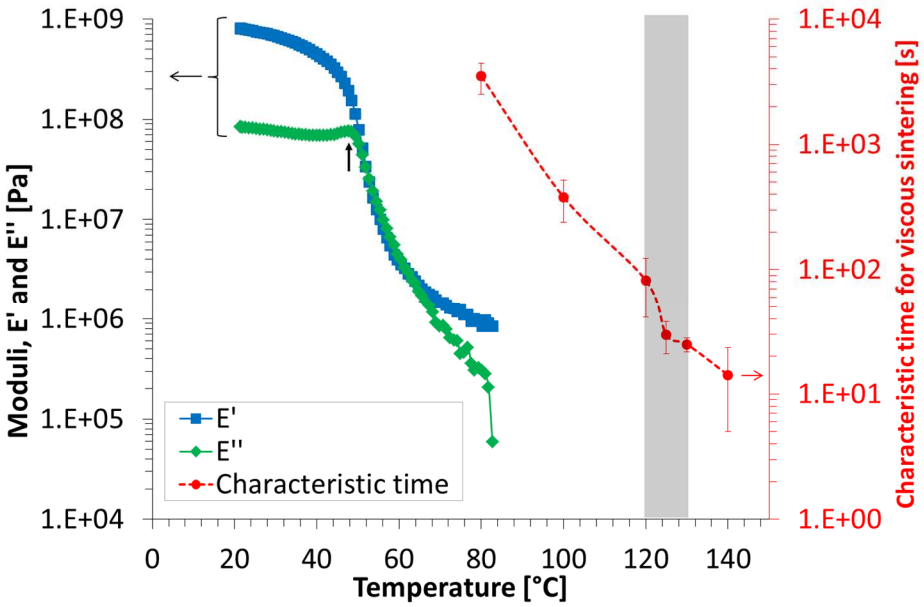

395

396 **Figure 7.** Chaunier *et al.*

Table 1. Fusion bonding properties of zein-based extruded filaments (average value ± standard deviation, for three replicates at each temperature set): Final bonding angle, final convexity index, measured values of bonding angle and bonding rate at 35s and estimated characteristic times for viscous sintering, t_{vs1} (issued from Eq.1; [6]) and t_{vs2} [9].

T_{set} [°C]	Final bonding angle, θ_{final} [rad]	Final convexity index, I_{Convex_final} [-]	θ at t=35s [rad]	dθ/dt at t=35s [10^{-4}rad.s^{-1}]	t_{vs1} (Eq.1) [s]	t_{vs2} (Hopper) [s]	$\frac{t_{vs\,1}}{t_{vs\,2}}$ [-]
80	0.39 ± 0.02	0.900 ± 0.011	0.31 ± 0.07	3.0 ± 0.8	5233 ± 1460	3492 ± 974	1.5
100	0.73 ± 0.14	0.917 ± 0.025	0.29 ± 0.03	28 ± 10.4	599 ± 222	380 ± 141	1.6
120	1.10 ± 0.10	0.972 ± 0.001	0.54 ± 0.21	108 ± 53.5	77 ± 38	82 ± 41	0.9
125	1.19 ± 0.05	0.987 ± 0.001	0.57 ± 0.05	294 ± 84.9	27 ± 8	30 ± 9	0.9
130	1.27 ± 0.01	0.989 ± 0.003	0.48 ± 0.04	364 ± 46.2	26 ± 3	25 ± 3	1.0
140	1.33 ± 0.27*	-	0.52 ± 0.11	625 ± 404.6	14 ± 9	14 ± 9	1.0

**High values of standard deviation at the completion of coalescence for T_{set}=140°C are due to the vaporization of the plasticizer creating bubbles and leading to the expansion of the material*

Graphical abstract

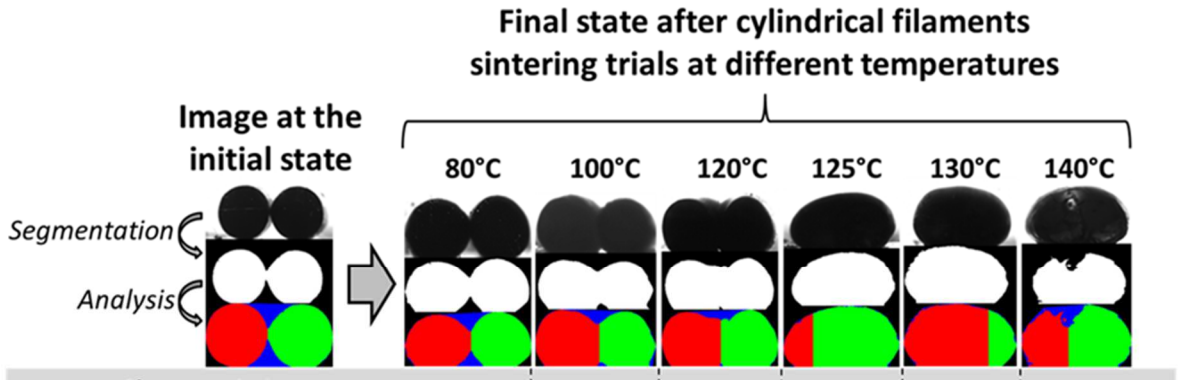

	80°C	100°C	120°C	125°C	130°C	140°C
Characteristic viscous sintering time [s] :	3492	380	82	30	25	*14 (bubbles)*
Final convexity index [-] :	0.900	0.917	0.972	0.987	0.989	-

Chaunier *et al.*